Electrically Pumped Whispering Gallery Mode Lasing from Au/ZnO Microwire Schottky Junction

*Sunayna B. Bashar, Chunxia Wu, Mohammad Suja, Hao Tian, Wenhao Shi, and Jianlin Liu**

Au/ZnO microwire Schottky diodes are fabricated. The devices exhibit typical Schottky diode *I–V* behavior with a turn-on voltage of about 0.72 V. The hexagonal ZnO microwires act as whispering gallery mode (WGM) lasing microcavities. Under forward bias, a three-microwire device exhibits WGM ultraviolet lasing spectra with a quality factor of about 1287. Output power of the laser has been measured at various injection currents, indicating threshold behavior with a threshold current of about 59 mA. Due to limited hole injection in the operation of Schottky diode, the lasing is a result of an excitonic recombination within the WGM cavity.

1. Introduction

Low-dimensional semiconductor micro/nanostructures gained a great deal of interest over the past two decades because they can in principle lead to higher-performance devices compared with their bulk counterpart. Owing to its wide bandgap (3.37 eV) and a large exciton binding energy (60 meV) which ensures excitons to exist at room temperature, zinc oxide (ZnO) is considered as a promising candidate for next-generation micro/nano ultraviolet (UV) optoelectronic devices, especially lasers.[1,2] Lasing actions from ZnO micro/nanostructures can originate from three mechanisms namely random,[3–7] Fabry–Perot (F–P),[8–10] and whispering gallery mode (WGM).[11–17] Random lasing is achieved by continuous scattering among ZnO grain boundaries or nanowire sidewalls. In the F–P type, 1D ZnO nano/microwires can act as individual lasing cavities with the naturally cleaved two end facets as mirrors. In WGM lasers, light propagates inside ZnO microstructures through consecutive total internal reflection (TIR) at the inner walls. As a result, WGM lasers are expected to have a high quality (Q) factor and a low threshold due to its low optical loss at the cavity boundary. Moreover, because of its excellent characteristics and resonance wavelength dependency on the surrounding medium, WGM lasers may find many important applications such as biosensors.[18–20] Therefore it is essential to develop WGM type of lasers. Thanks to the inherent wurtzite structure, high-quality hexagonal ZnO microstructures of various sizes can be readily grown by using relatively simple approaches such as vapor phase transport method and serve as excellent WGM lasing cavities. However, most efforts on WGM ZnO microlasers are based on optical pumping,[11–15] and electrically pumped WGM lasers are rarely reported.[16,17] Among these electrically pumped WGM laser efforts,[16,17] the devices are based on heterojunctions involving n-type ZnO and a p-type dissimilar material because p-type ZnO is difficult to achieve and unstable,[21] and lasing mechanism is explained by excitonic recombination. As a matter of fact, excitonic lasing has also been observed in random lasers made of various types of structures including metal–insulator–semiconductor (MIS) structure, metal–semiconductor Schottky junction, and metal–semiconductor–metal (MSM) junction.[5,6,22] Because of the involvement of excitonic recombination process, these devices operate with hole carrier injection much less than Mott density, therefore population inversion is not necessary in contrast to the electron–hole plasma (EHP) lasing, which definitely requires a p–n junction.[23] In the present work, we report excitonic lasing based on Au/ZnO microwire WGM Schottky laser diodes. Electroluminescence (EL) characteristics and lasing mechanism have been investigated in detail.

2. Results and Discussion

2.1. Structural and Optical Characterizations

ZnO microwires were synthesized by vapor phase transport method. The detailed growth conditions are given in the Experimental Section. **Figure 1**a shows a scanning electron microscopy (SEM) image of as grown ZnO microwires. The length and diameter of the microwires is around 0.2–3 mm and 8–12 μm, respectively. Figure 1b shows a SEM image of an individual microwire viewed from its side, indicating smooth hexagonal facets of the microwire. This morphology is important for establishing TIR inside the wires, which act as WGM microcavity. It is also evident from the SEM images that microwires have been grown along the *c*-axis. Figure 1c shows an X-ray diffraction

S. B. Bashar, M. Suja, H. Tian, W. Shi, Prof. J. Liu
Department of Electrical and Computer Engineering
University of California at Riverside
Riverside, CA 92521, USA
E-mail: jianlin@ece.ucr.edu
Dr. C. Wu
School of Materials Science and Engineering
Jiangsu University
Jiangsu 212013, China

DOI: 10.1002/adom.201600513

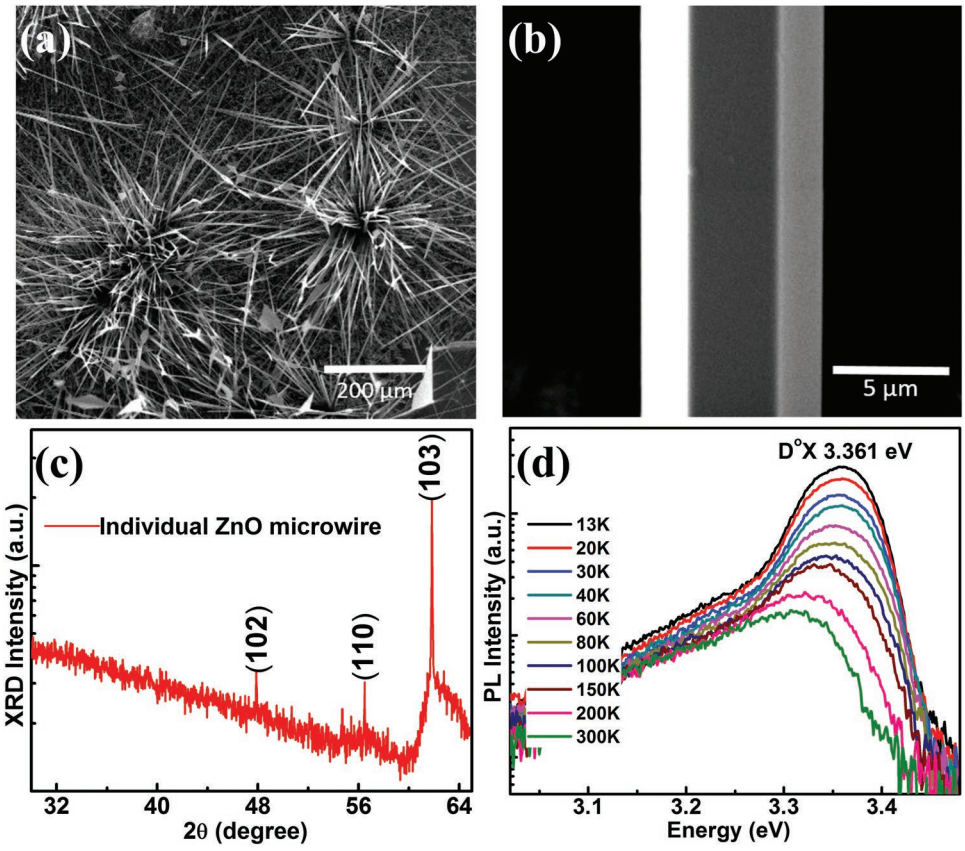

Figure 1. a) SEM image of as-grown ZnO microwires, b) SEM image, c) XRD spectrum of an individual ZnO microwire, and d) temperature-dependent PL spectra of ZnO microwires.

(XRD) pattern of an individual ZnO microwire, which is horizontally placed on a substrate. The spectrum exhibits diffraction peaks from ZnO(102), ZnO(110), and ZnO(103) planes, indicating the hexagonal wurtzite crystal structure and *c*-axis growth of this ZnO microwire.[24] Figure 1d shows temperature-dependent photoluminescence (PL) spectra of ZnO microwires under the temperatures between 13 and 300 K. The dominant peak at 3.361 eV is usually observed in the undoped n-type ZnO and can be attributed to the donor bound exciton (D°X) emission. As the temperature is increased gradually, D°X-associated emissions dissociate into free exciton (FX) related emissions. Therefore, it is supposed that FX-related emissions dominate at room temperature.[25] Additionally, the emission peaks shift to lower energy with the increase of temperature due to the fact that the bandgap decreases with the increase of temperature.

2.2. Electrical Characterization

Left inset of **Figure 2** shows a schematic diagram of the cross-sectional view of the Au/ZnO microwire Schottky junction WGM laser device. Step-by-step fabrication processes are summarized in the Experimental Section. Bottom right inset of Figure 2 shows an optical microscopy image of three microwires, having similar diameters, which were assembled as the active region of the device. Current–voltage (*I*–*V*) curve in Figure 2 demonstrates rectifying behavior with a turn-on voltage of about 0.72 V. Since Au has a work function of ≈5.1 eV and the electron affinity of ZnO is ≈4.35 eV, Schottky junction with a Schottky barrier of ≈0.75 eV is expected to be formed between them. This low turn-on voltage from the device

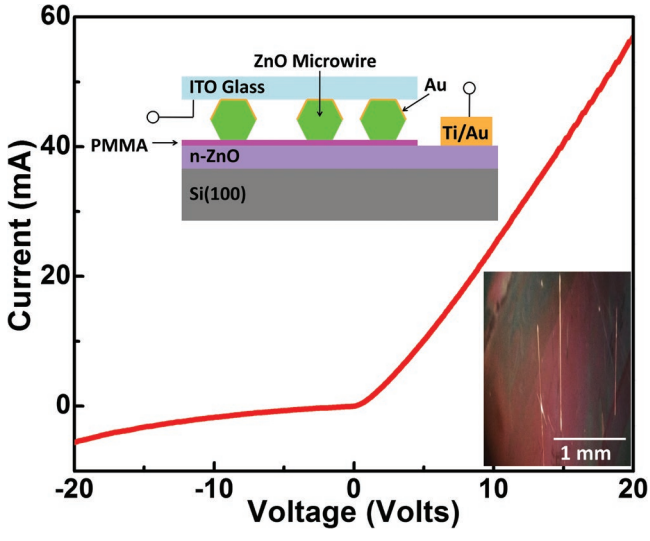

Figure 2. *I*–*V* characteristic of a three-microwire-based device. Left inset shows a schematic diagram of the cross-sectional view of Au/ZnO microwire Schottky diode laser. Bottom right inset shows an optical microscope image of the three micowires after being transferred.

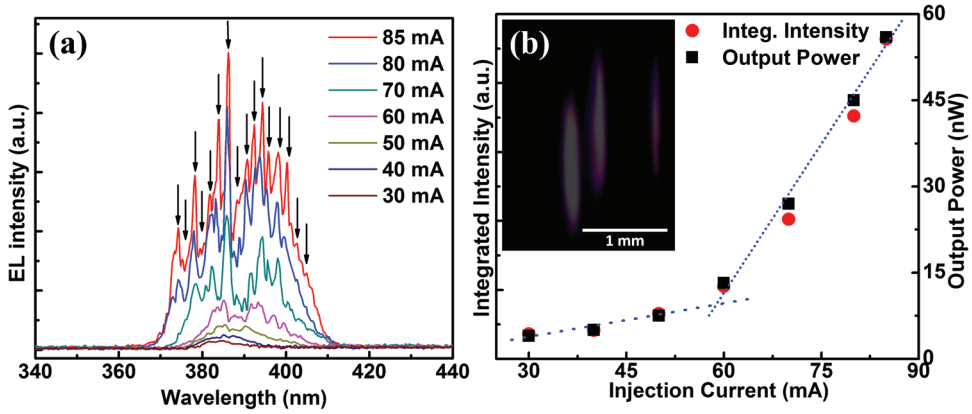

Figure 3. a) Emission spectra of the diode under different injection currents. Arrows represent WGM lasing modes, b) integrated intensity and output power as a function of injection current, inset shows far-field emission pattern of the device at a current of 85 mA.

confirms this fact.[26] A device with two ZnO microwires was also fabricated and characterized, showing similar Schottky diode *I–V* characteristic with a turn-on voltage of ≈0.75 V (Figure S1a, Supporting Information).

2.3. Lasing Characterization

Figure 3a shows room temperature EL emission spectra of the three-microwire Schottky junction laser device at different forward currents. The EL emission band extends from 370 to 410 nm. At a forward current of 30 mA, a broad spontaneous emission band centered around 384 nm can be seen. With increasing forward currents to, e.g., 40 and 50 mA, the intensity of spontaneous emission bands increases. At injection currents above 50 mA, several discrete peaks emerge in the spontaneous emission spectrum, indicating a change from spontaneous emission to stimulated emission. As the forward current increases to 85 mA, many sharp lasing peaks with a full-width at half maximum (FWHM) of about 0.3 nm appear in the spectrum, which implies that there is enough gain to sustain cavity modes in ZnO microwires. The Q factor is estimated to be about 1287, according to $Q = \frac{\lambda}{\partial\lambda}$, where λ and $\partial\lambda$ are the peak wavelength (386 nm) and FWHM (0.3 nm), respectively. Since we have only three wires reasonably apart from each other, random lasing is not possible because random lasing requires a large number of randomly distributed scattering sites in a medium. Also the probability of F–P lasing from opposite facets is excluded considering the fact that it would result in very weak optical confinement with much lower Q factor. Therefore, WGM is the dominant feedback mechanism in our structure.[13]

Mode spacing of a WGM laser can be determined by the following equation:

$$\Delta\lambda = \frac{\lambda^2}{Ln\left(1 - \frac{\lambda}{n}\frac{dn}{d\lambda}\right)} \approx \frac{\lambda^2}{Ln_{ZnO}}$$

where λ is the peak wavelength (386 nm), n is the refractive index of ZnO ($n_{ZnO} \approx 2.45$), and L is the cavity length. The cavity length is assumed to be maximum possible optical path traversed by light inside these hexagonal cavities, which is ≈3 × *D*. *D* is diameter of the microwire or twice of the edge length of the hexagonal cross section. The three wires in the device have similar diameters of around 8 µm. These wires are quite apart from each other and can be considered as individual functioning cavities. Therefore, the mode spacing is estimated to be about 2.53 nm. Furthermore, since the emission bandwidth is roughly 40 nm as shown in Figure 3a, the number of WGM modes is about 15. These results are in close agreement with experimentally observed values from Figure 3a. The EL spectra of a two-wire device show a similar WGM lasing mode structure, which has a free spectral range of about 2.05 nm as a result of a larger diameter (Figure S1b, Supporting Information). Angle-dependent EL measurement of the three-wire device further proves the WGM lasing characteristics (Figure S2, Supporting Information).

Figure 3b shows integrated intensity and output power as a function of forward injection currents. The integrated intensity is the integral of all area under the EL curve, which is equivalent to total output power for emissions at all wavelengths. The output power is measured real time from the device for one particular lasing mode. In this case the power was measured at a wavelength around the ZnO near band edge emission, i.e., 386 nm. As seen from the graph, both have similar trend: they increase slowly as the injection current is below ≈50 mA, and increase rapidly as the injection current increases beyond ≈50 mA. By interpolating the data points, the lasing threshold is estimated to be around 59 mA. The output power is measured as 56 nW at an injection current of 85 mA. The inset of Figure 3b shows a far-field emission pattern, indicating blue-violet light emission from the three-microwire based laser device at an injection current of 85 mA. A device using two ZnO microwires as the lasing cavity shows similar threshold behavior (inset of Figure S1b, Supporting Information).

2.4. Discussion

Figure 4a–c shows energy band diagrams of Au/ZnO microwire Schottky laser diode at thermal equilibrium, moderate forward

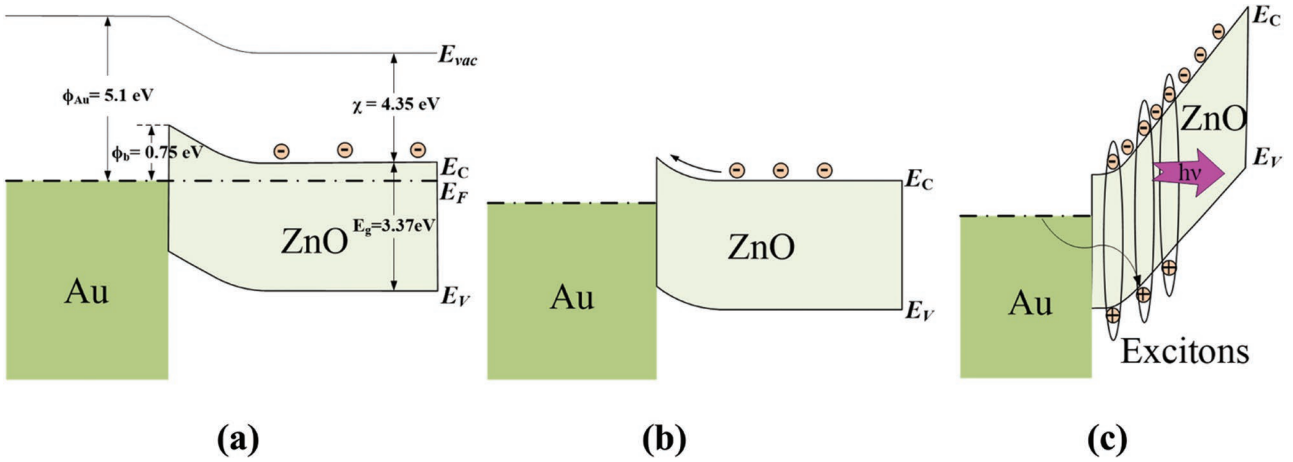

Figure 4. Band diagram of Au/ZnO Schottky junction under a) equilibrium condition, b) forward bias on the Au metal, and c) strong forward bias on the Au metal.

bias, and strong forward bias, respectively. Values for relevant parameters such as bandgap, metal work-function, electron affinity, barrier height are illustrated. Due to a Schottky barrier of about 0.75 eV, thermionic emission of electrons across the barrier is relatively small and balanced at equilibrium. Under moderate forward bias on the Au metal, the ZnO band shifts upward, leading to a lower energy barrier for electrons. As strong forward bias is applied, the ZnO band bends sharply, leading to a narrower triangular energy barrier for holes at the Au/ZnO junction. Thus, while there is a continuous flow of large number of electrons toward Au contact, which contribute to the major portion of diode current, the holes from the positive battery pole via Au electrode can tunnel into the valence band of ZnO directly or through trap-assisted tunneling to form a small hole current. Since the electrons and holes are flowing in the opposite direction, there are ample probabilities for them to couple with each other and form excitons.[27,28] These excitons then recombine to emit light almost instantaneously.[28] It should be noted that this device is different with the MIS laser device, where a large barrier at the metal–semiconductor interface is used to confine electrons in the semiconductor for lasing as reported by Zhu et al.[4] Considering the fact that Schottky diode is a majority carrier device and there is very limited hole supply to the junction during operation, lasing phenomena should originate from excitonic recombination as opposed to EHP. As a matter of fact, EHP lasing would require a population inversion condition, which could not be established in a Schottky diode. On the other hand, since excitonic lasing does not require population inversion, it accounts for the observed lasing phenomenon.[6,23] High-temperature EL measurements were performed to further prove the lasing being excitonic emission in these devices (Figure S3, Supporting Information).

3. Conclusion

Hexagonal ZnO microwires were synthesized by vapor phase transport method. Electrically pumped WGM lasing was achieved from simple device structures based on Au/ZnO microwire Schottky junctions. The origin of the lasing is ascribed to excitonic recombination in WGM cavities. Although the present laser, which consists of two or three far-apart placed microwires are multimode UV lasers, this work takes an important step toward more advanced WGM lasers such as single wire lasers and coupled-mode ZnO microwire WGM Schottky diode lasers with higher mode purity.

4. Experimental Section

Microwire Growth: ZnO microwires were grown in an Atmospheric Pressure Chemical Vapor Deposition (APCVD) by employing vapor phase transport mechanism. First, a horizontal tube furnace was set to heat up to 1150 °C. Then, a mixture of ZnO and graphite powder (mass ratio 1:1) was loaded into a quartz boat and a Si substrate was placed upside down on top of the boat. As the furnace reached its set temperature value, the boat with the substrate was inserted inside the furnace and kept there for 30 min. Microwires were grown directly onto the Si substrate.

ZnO Thin Film Growth: A high-quality *c*-axis oriented undoped ZnO thin film was grown on a MgO buffer layer on Si(100) using an SVT Associates (SVTA) radio frequency (RF) plasma-assisted molecular beam epitaxy (MBE) system. The Si wafer was first cleaned by a standard RCA procedure and then the 4 nm MgO buffer film was grown for 5 min with a Mg cell temperature of 450 °C and an O_2 flow rate of 1.5 sccm at a substrate temperature of 400 °C. It was then followed by the growth of a ZnO thin film layer of around 500 nm with a Zn cell temperature of 340 °C and an O_2 flow rate of 2 sccm for 4 h at 500 °C.

Device Fabrication: Au/ZnO microwire Schottky junction WGM lasers were fabricated using the following process. First, polymethyl methacrylate (PMMA) was spin-coated on ZnO thin film layer for 45 s under a speed of 6000 rpm producing a film of ≈50 nm. Then, the microwires were picked out by a tweezer and placed horizontally on the ZnO layer with the help of PMMA. This transfer was then followed by a post bake for 80 s at 110 °C to drive off the solvents from PMMA and secure the microwires in place. PMMA serves several purposes in this structure. First, it works as an adhesive to fix the wires in place. Second, it isolates the top metal contact from being electrically shorted. Third, it improves the reflection at the lower facet of ZnO microwire compared with a scheme that the wire is directly contacted on ZnO. Finally, 5 nm Au and 10/100 nm Ti/Au metals were e-beam evaporated on ZnO micorwires and ZnO layer, respectively, to form contacts. An indium tin oxide (ITO) glass slide (≈15–25 Ω sq^{-1}) was placed on top of the Au contact for reliable current feed through during electrical measurements (inset of Figure 2).

Structural, Optical, Electrical, and Luminescence Characterizations: SEM images were taken using a Philips XL 30 SEM system. X-ray diffraction measurement was performed using a Bruker D8 Advance X-ray diffractometer. A home built PL system consisting of a Kimmon Koha 325 nm He-Cd laser, a Janis cryostat, an Oriel monochromator, a lock-in amplifier equipped with a chopper and a photomultiplier tube were used to measure PL from ZnO microwires. *I–V* curves were measured through a Signatone Probe Station (Model H150) connected to a Semiconductor Parameter Analyzer (Agilent 4155C). EL measurement makes use of almost similar system as the PL measurement except that an external DC power supply (HP E3630A) was used as the excitation source instead of the He-Cd laser. A Thorlabs PM100 optical power meter was used for measuring output power from the devices.

Supporting Information

Supporting Information is available from the Wiley Online Library or from the author.

Acknowledgements

Thin film growth, device fabrication, and characterization were supported as part of the SHINES, an Energy Frontier Research Center funded by the US Department of Energy, Office of Science, Basic Energy Sciences under Award No. SC0012670. Growth of ZnO microwires was supported by China Scholarship Council and National Natural Science Foundation of China (11304127).

Received: July 1, 2016
Revised: July 27, 2016
Published online: September 4, 2016

[1] M. H. Huang, S. Mao, H. Feick, H. Yan, Y. Wu, H. Kind, E. Weber, R. Russo, P. Yang, *Science* **2001**, *292*, 1897.
[2] X. Wang, C. J. Summers, Z. L. Wang, *Nano Lett.* **2004**, *4*, 423.
[3] J. Huang, S. Chu, J. Y. Kong, L. Zhang, C. M. Schwarz, G. P. Wang, L. Chernyak, Z. H. Chen, J. L. Liu, *Adv. Opt. Mater.* **2013**, *1*, 179.
[4] H. Zhu, C. X. Shan, J. Y. Zhang, Z. Z. Zhang, B. H. Li, D. X. Zhao, B. Yao, D. Z. Shen, X. W. Fan, Z. K. Tang, X. Hou, K. L. Choy, *Adv. Mater.* **2010**, *22*, 1877.
[5] X. Ma, J. Pan, P. Chen, D. Li, H. Zhang, Y. Yang, D. Yang, *Opt. Express* **2009**, *17*, 14426.
[6] F. Gao, M. M. Morshed, S. B. Bashar, Y. Zheng, Y. Shi, J. Liu, *Nanoscale* **2015**, *7*, 9505.
[7] H. K. Liang, S. F. Yu, H. Y. Yang, *Appl. Phys. Lett.* **2010**, *97*, 241107.
[8] S. Chu, G. Wang, W. Zhou, Y. Lin, L. Chernyak, J. Zhao, J. Kong, L. Li, J. Ren, J. Liu, *Nat. Nanotechnol.* **2011**, *6*, 506.
[9] J. C. Johnson, H. Yan, P. Yang, R. J. Saykally, *J. Phys. Chem. B* **2003**, *107*, 8816.
[10] H. Yan, R. He, J. Johnson, M. Law, R. J. Saykally, P. Yang, *J. Am. Chem. Soc.* **2003**, *125*, 4728.
[11] C. Czekalla, C. Sturm, R. Schmidt-Grund, B. Cao, M. Lorenz, M. Grundmann, *Appl. Phys. Lett.* **2008**, *92*, 241102.
[12] J. Dai, C. X. Xu, K. Zheng, C. Z. Lv, Y. P. Cui, *Appl. Phys. Lett.* **2009**, *95*, 241110.
[13] R. Chen, B. Ling, X. W. Sun, H. D. Sun, *Adv. Mater.* **2011**, *23*, 2199.
[14] G. P. Zhu, C. X. Xu, J. Zhu, C. G. Lv, Y. P. Cui, *Appl. Phys. Lett.* **2009**, *94*, 051106.
[15] J. Dai, C. X. Xu, P. Wu, J. Y. Guo, Z. H. Li, Z. L. Shi, *Appl. Phys. Lett.* **2010**, *97*, 011101.
[16] J. Dai, C. X. Xu, X. W. Sun, *Adv. Mater.* **2011**, *23*, 4115.
[17] G. Y. Zhu, J. T. Li, Z. S. Tian, J. Dai, Y. Y. Wang, P. L. Li, C. X. Xu, *Appl. Phys. Lett.* **2015**, *106*, 021111.
[18] X. F. Jiang, C. L. Zou, L. Wang, Q. Gong, Y. F. Xiao, *Laser Photon. Rev.* **2016**, *10*, 40.
[19] L. He, Ş. K. Özdemir, L. Yang, *Laser Photon. Rev.* **2013**, *7*, 60.
[20] X. F. Jiang, Y. F. Xiao, C. L. Zou, L. He, C. H. Dong, B. B. Li, B. B. Li, Y. Li, F. W. Sun, L. Yang, Q. Gong, *Adv. Mater.* **2012**, *24*, OP260.
[21] D. C. Look, B. Claflin, *Phys. Status Solidi B* **2004**, *241*, 624.
[22] M. M. Morshed, M. Suja, Z. Zuo, J. Liu, *Appl. Phys. Lett.* **2014**, *105*, 211107.
[23] J. W. Sun, Y. M. Lu, Y. C. Liu, D. Z. Shen, Z. Z. Zhang, B. H. Li, J. Y. Zhang, B. Yao, D. X. Zhao, X. W. Fan, *J. Phys. D: Appl. Phys.* **2008**, *41*, 155103.
[24] O. Lupan, L. Chow, G. Chai, B. Roldan, A. Naitabdi, A. Schulte, H. Heinrich, *Mater. Sci. Eng. B* **2007**, *145*, 57.
[25] S. Xu, W. Guo, S. Du, M. M. T. Loy, N. Wang, *Nano Lett.* **2012**, *12*, 5802.
[26] M. Asghar, K. Mahmood, M. Faisal, M. A. Hasan, *JPCS* **2013**, *439*, 012030.
[27] P. G. Kasherininov, A. V. Kichaev, A. A. Tomasov, *Semiconductors* **1995**, *29*, 1092.
[28] H. Jeong, K. Min, S. Byun, C. J. Stanton, D. H. Reitze, J. K. Yoo, G. C. Yi, Y. D. Jho, *Appl. Phys. Lett.* **2012**, *100*, 092106.